ACS OMEGA

Open Access

http://pubs.acs.org/journal/acsodf

Article

In Silico Study of a Small Bioactive Molecule Targeting Topoisomerase II and P53-MDM2 Complex in Triple-Negative Breast Cancer

Vishal Singh, Suman Verma, Fiza Fatima, Sintu Kumar Samanta, Pritish Kumar Varadwaj,* and Amaresh Kumar Sahoo*

Cite This: *ACS Omega* 2023, 8, 38025−38037

Read Online

ACCESS | Metrics & More | Article Recommendations | Supporting Information

ABSTRACT: Treatment of triple-negative breast cancer (TNBC) is very challenging as only few therapeutic options are available, including chemotherapy. Thus, a constant search for new and effective approaches of therapy that could potentially fight against TNBC and mitigate side effects is "turn-on". Recently, multitarget therapy has come up with huge possibilities, and it may possibly be useful to overcome several concurrent challenges in cancer therapy. Herein, we proposed the inhibition of both Topoisomerase II enzyme and p53-MDM2 (p53 cavity in MDM2) protein complex by the same bioactive molecules for multitarget therapy. RNA-seq analysis was performed to get a network of essential proteins involved in the apoptosis pathway by considering the triple-negative breast cancer cell line (MDA-MB-231). All of the untreated duplicate sample data were retrieved from NCBI (GSC149768). Further, via *in silico* screening, potent bioactive molecules were screened out to target both Topo II and the p53-MDM2 complex. The results of ligand-based screening involving docking, MMGBSA, ADME/T, MD simulation, and PCA suggested that resveratrol, a plant bioactive molecule, showed more potential binding in the same cavity of target proteins compared with doxorubicin for Topo II*α* (5GWK) and etoposide for the second protein target (p53-MDM2 complex; 4OQ3) as the control drug. This is also evident from the in vitro validation in case of triple-negative breast cancer cell lines (MDA-MB-231) and Western blotting analysis. Thus, it paves the scope of multitargeting against triple-negative breast cancer.

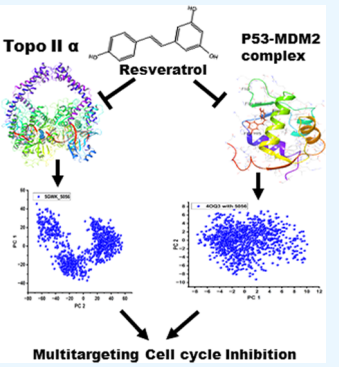

1. INTRODUCTION

Breast cancer is one of the leading causes of death globally owing to its diversity and rapid rate of mutations that lead to change in its characteristics very fast; thus, in several cases common therapeutics could not produce desired outcomes. About 10−15% of all breast cancers are called triple-negative breast cancers (TNBCs) as this breast cancer subtype does not have progesterone and estrogen hormone receptors (PR or ER), and HER2 overexpression too.[1−3] This type of cancer cell is generally aggressive as it grows more rapidly. It would be worth mentioning here that only few systemic treatment options are available along with chemotherapy (CT) to treat the TNBCs.[1−5] The 'single drug and single target' approach does not provide great success. Moreover, eradication of the resistant cancer cells is a major challenge, where multitarget therapeutics might offer better option as it concurrently inhibits several cellular pathways and thus becomes more lethal toward cancer cells. However, choice of drugs that are "selectively specific" and understanding the mechanism of the actions at molecular level are very essential prior to any *in vivo* applications of multitarget therapy.[6−11] In this regard, high-throughput virtual screening (HTVS) is found to be very beneficial, which provides a fast and cost-effective method of screening of lead molecules. This also provides an idea about the molecular mechanism of the action of each drug molecule. Furthermore, along with the *in silico* screening, successful clinical outcomes of multitarget therapy and combination drug therapy have also delivered enough assurance to judiciously opt for a suitable lead molecule for targeting more than one pathway. Similarly, there have been lots of recent research activities going on to find out novel inhibitors of important proteins (e.g., enzyme) in cancer therapy, such as topoisomerase enzymes involved in apoptosis/cell growth.[12] For the last few decades, a wide range of anticancer drug molecules have been reported, which have different biomacromolecules as target sites. However, cancer therapeutics primarily targeting DNA directly or indirectly by means of some enzymes associated with DNA are found to be very potential owing to the poor DNA repair machinery of the cancer cells as compared to the normal cells. Several conventional chemotherapeutics as well as radiation therapies exploit this strategy and are being utilized as prospective cancer therapeutic agents

Received: May 24, 2023
Accepted: September 11, 2023
Published: October 3, 2023

https://doi.org/10.1021/acsomega.3c03640
ACS Omega 2023, 8, 38025−38037

Scheme 1. Schematic Pipeline of the Methods Followed in the Study

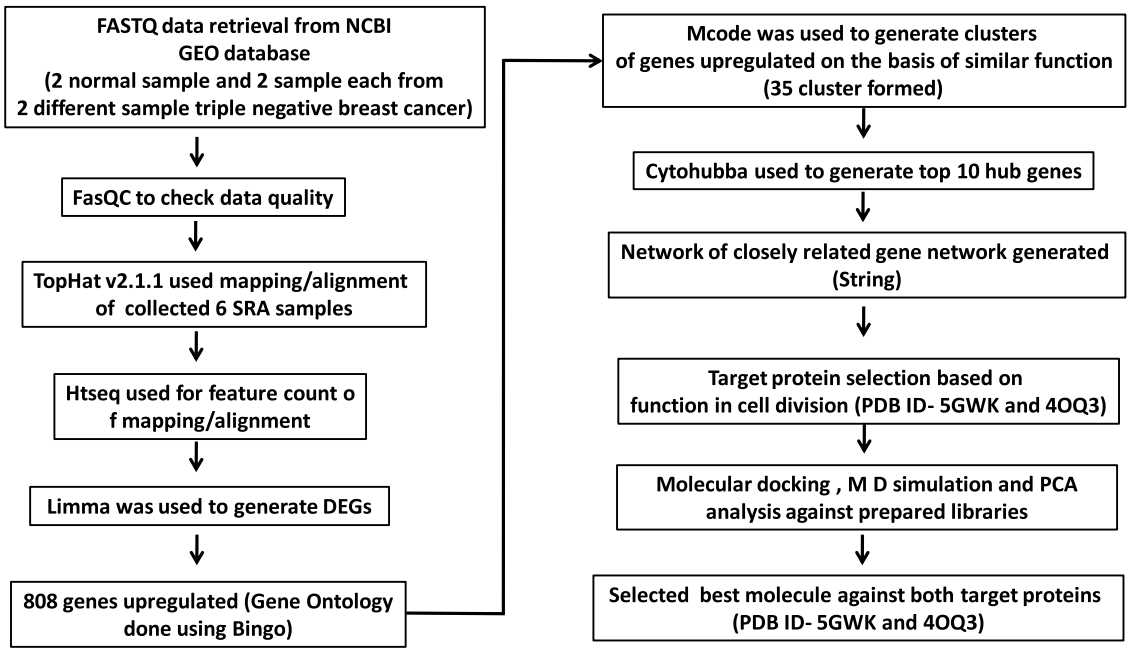

due to their effective outcomes. Likewise, topoisomerase IIα has been the most preferred therapeutic target for cancer therapy nowadays[13] as it is found in increased amount in cancerous cells.

Topoisomerase II has two subclasses: one, topoisomerase IIα, is a homodimer, whereas the other, topoisomerase IIβ, has a heterotetrametric structure.[14] Both the isoforms are structurally ∼70% identical considering the amino acid sequence. Topoisomerase IIα is required for all growing cells and the concentration of the enzyme reaches the highest level during the G2/M phase of the complete cell cycle.[15,16] Moreover, topoisomerase IIα plays a significant role in the movement of the replication fork and chromosome segregation during mitosis. Hence, the active function of topoisomerase IIα plays a significant role in cell division and its survival.[16,17] Topoisomerase II inhibitors are used as chemotherapeutic agents due to their ability to induce tumor cell death.[18] Another protein that is significant in cancer therapy is the guardian of the gene p53. The role of P^{53} is well known: that it is important in controlling the cell cycle and apoptosis. P^{53} cannot express in several cancerous cells and is found in a large amount as mutant P^{53}. On the MDM2 protein is present a product of one of the responsive genes of P^{53}. As stated by the recent research groups,[19] MDM2 interacts and binds with P^{53} protein, and the function of P^{53} is inhibited via three major steps: (1) MDM2 ubiquitinates P^{53} through its E3 ligase activity, which therefore promotes proteasomal degradation of P^{53}; (2) P^{53} and MDM2 interaction blocks the P^{53} from binding to its targeted DNA, hence blocking P^{53}'s transcriptional activity; and (3) export of P^{53} is facilitated by MDM2 out of the nucleus, making P^{53} inaccessible to the DNA and therefore minimizing/reducing its transcriptional ability. Therefore, it ultimately provides a P^{53}-MDM2 autoregulatory feedback loop. Nonfunctional P^{53} leads to development as well as progression of tumor cells. One study shows the effect of Topoisomerase II inhibitors on the autoregulatory feedback loop of the P^{53}-MDM2 complex, which suggests an involvement of Topoisomerase II in P^{53} regulation.[18] This is done by activating the G1 checkpoint and P^{53}–P^{21} pathway.[20] One of the reasons for cancer progression is the faster rate of mutation with time (more than 50%) along with increased expression of MDM2.[21] This has led to numerous evaluations and investigations of its role and potential as a therapeutic target in the sense of restoring wild-type P^{53}.

As observed by already known drugs of topoisomerase II inhibitors (e.g., doxorubicin), cytotoxic concentrations are needed for inhibiting the P^{53}-MDM2 autoregulatory feedback loop.[22] In this study, we analyzed untreated SRA data (normal/cancer in doublet) retrieved from NCBI to generate an upregulated proteins and associated proteins network based on function. On the basis of their function and significance in cell division/arrest, we selected two proteins as targets. Considering the hypothesis that topoisomerase II inhibitor (screened lead bioactive molecule) will restrain DNA uncoiling, resulting in cell arrest and activation of P53 and simultaneously interacting with p53 binding cavity of MDM2 at the same dose, this can probably be used as an effective therapeutic approach to stimulate cell arrest and further apoptosis. This single-drug-multitarget approach targets two or more pathways with a lower or same drug concentration, unlike before, where more cytotoxic concentration was needed for activating the P^{53} apoptosis pathway than for the inhibition of Topoisomerase II.[18] Drugs approved by the library of natural compounds, FDA, and drugs from NCI database were prepared and *in silico* screening for determining the interaction of each compound with the P^{53}-MDM2 complex (PDB ID—4OQ3) and Topoisomerase II (PDB ID—5GWK) was done. Compounds thus shortlisted from each library showed better binding energy with both the P^{53}-MDM2 complex and Topoisomerase IIα when compared with control drugs.

2. MATERIALS AND METHODS

2.1. Overall Method. The *in silico* study involves appropriate tools and a pipeline of techniques usually applied to Sequence Read Archive (SRA) data analysis to generate differentially expressed genes (DEGs) and important hub gene

https://doi.org/10.1021/acsomega.3c03640
ACS Omega 2023, 8, 38025−38037

networks involved in various cellular/molecular functions, and for structure-based high-throughput screening. In this study, target protein preparation and grid generation, library preparation, and screening out the best ligands on the basis of dock score, ADME/T, and MMGBSA scores were done using Glide v8.3 Schrodinger, LLC, New York, NY, 2020-4. Furthermore, MD simulation study and PCA analysis of the best-screened protein−ligand complex were done and compared with the control drugs (doxorubicin and etoposide) using Schrodinger, LLC, New York, NY, 2019-1. The workflow of our study is briefly illustrated in Scheme 1.

2.2. Data Retrieval and Preprocessing. The original data are available at NCBI (https://www.ncbi.nlm.nih.gov/gds) Gene Expression Omnibus (GEO) under accession number GSE149768. The RNA-Seq reads have been extracted from the SRA files and converted into FASTQ file format. All of the SRA data collected for analysis are untreated as (a) SRR116682386 and SRR116682387 from the MCF 10 cell line, (b) SRR116682394 and SRR116682395 from the MCF 7 cell line, and (c) SRR116682402 and SRR116682403 from the MDA-MB 231 cell line. The quality of the RNA data retrieved was analyzed by FastQC (http://www.bioinformatics.babraham.ac.uk/projects/fastqc). Sequencing incorrect nucleotides, GC content, and phred score were analyzed using this tool.[23]

2.3. Sequence Alignment and Differential Gene Expression Analysis. TopHat (v2.1.1) is designed to deal with aligning the reads of target nucleotide sequences with the reference genome sequence using the Bowtie aligner algorithm. It assembles the mapping of reads to generate consensus sequences using reference sequences (normal/control). It generates various splice junctions with the help of a known acceptor/donor junction. Further, the htseq-count script, a part of the HTSeq module, was used via the htSeq tool using an SAM or BAM alignment file to generate the feature count.

This procedure was carried out for all of the untreated and treated sample replicates. Limma was used for analyzing differentially expressed genes (DEGs). It takes the count file as an input generated from the Htseq-count algorithm. The cutoff score for fold enrichment for selected upregulated genes was >2 and p-value <0.1 was selected.

2.4. Gene Ontology Analysis and Target Identification. All of the DEGs were imported to Cytoscape and used plugins such as Bingo and cytohubba for hub genes network generation. Bingo database and server were used for gene ontology of all upregulated genes from the total DEGs. To generate clusters of genes we used Mcode, and for hub genes network we used Cytohubba.[24,25]

2.5. Ligand Collection and Library Preparation. The libraries of anticancerous biomolecules as ligands were collected from different databases such as the National Cancer Institute (376 ligands) (v), drugs used for lung cancer (35 ligands), FDA-approved drugs (70 molecules), and also from previous research papers, viz. fruits, vegetables, and spices (698 molecules). All of the ligands were downloaded from PubChem and were subjected to LigPrep, Glide v8.3 Schrodinger, LLC, New York, NY, 2020-4 to yield different stable conformations of all 1179 ligands for docking under the default condition of LigPrep/Epik.

2.6. Protein Preparation and Grid Generation. 5GWK and 4OQ3 were downloaded from the protein data bank (RCSB PDB). Default parameters of protein preparation (Glide, Maestro v12.0, Schrodinger, LLC, New York, NY, 2020-4) were applied. A grid was generated around the predicted binding sites using PDBsum. The dimensions of the outer box were kept as $X = 36$, $Y = 36$, and $Z = 36$; those of the inner box as $X = 30$, $Y = 30$, and $Z = 30$; those of the grid center near Glu 461, Gly 463, Arg 487, Asp 543, Asp541, and Met 766 as $X = -6.24$, $Y = 52.23$, and $Z = 68.69$ for 5GWK and for 4OQ3; those of our second-target outer box as X = 25, $Y = 25$, and $Z = 25$; those of the inner box as $X = 20$, $Y = 20$, and $Z = 20$; and those of the grid center kept around HIS961, LYS94, LEU54, GLY58, ILE61, MET62, and TYR67 as $X = 13.99$, $Y = -20.8$, and $Z = 6.75$ using Glide v8.3, Schrodinger, LLC, New York, NY, 2020-4.

2.7. Structure-Based Virtual Screening Studies. In the present study, structure-based docking was performed using Glide v8.3, Schrodinger, LLC, New York, NY, 2020-4 in order to evaluate the docking score of all of the prepared libraries against the target proteins (5GWK and 4OQ3). Ligands' conformation with the best docking score was considered for further screening and evaluation against both the target proteins. Docking score is a cumulative score of different energies/interactions such as van der Waals energy, Coulomb energy, lipophilic term, hydrogen bond term, metal binding term, rewards, and penalties. Here we have taken doxorubicin as the control for topo IIα (5GWK) and etoposide for the second protein target (p53-MDM2 complex; 4OQ3). Docking/MMGBSA scores of doxorubicin (docking score: −7.271 kcal/mol, MMGBSA score: −38.41 kcal/mol) were considered as the screening cutoff score for ligands against 5GWK, whereas docking/MMGBSA scores of etoposide (docking score: −4.853 kcal/mol, MMGBSA score: −50.52 kcal/mol) were kept as the screening cutoff for 4OQ3.

2.8. ADME/T Property Prediction (Absorption, Distribution, Metabolism, Excretion, and Toxicity). ADME/T calculation is essential for any ligand to be considered/screened as a lead molecule. The druggable properties like Mol•wt, dipole moment, SASA, FOSA, FISA, PISA, QP LogS, CIQP LogS, QP Log HERG, QPcaco, QP Log BB, and QPPMDCK were calculated using QikProp-V6, Glide v8.3, Schrodinger, LLC, New York, NY, 2020-4.

2.9. Binding Energy Estimation through MMGBSA. The binding energy estimations were calculated further using Prime, Glide v8.3, Schrodinger, LLC, New York, NY, 2020-4. The scores estimated/calculated are the different binding affinities like dG bind, dG Bind Coulomb, dG Bind Covalent, dG Bind H bond, and dG Bind Solv. of the docked complex following the default prime condition.

2.10. Molecular Dynamics Simulation Study. For MD simulation, the system building of the protein−ligand complex was done using a system builder, and a solvent model with a water orthorhombic box TIP3P around the complex was performed. The dimensions of the box were chosen such as to cover the complex completely, providing the real environment for molecular dynamics simulation. MD simulation was done using Desmond, Schrodinger, LLC, New York, NY, 2019-1 to evaluate the stability of the protein−ligand complex. Complex RMSD, complex contact bar graph, and root-mean-square fluctuation (RMSF) were analyzed to assess the stability of the protein−ligand complex throughout the 100 ns simulation. Further, the box generated by the system was energy minimized and the charges of the water solution were neutralized by adding Na^+ and Cl^- ions with a default concentration of 0.15 M. The standard temperature (300.0 K) and standard pressure (1.01325 bar) were kept default for the

https://doi.org/10.1021/acsomega.3c03640
ACS Omega 2023, 8, 38025−38037

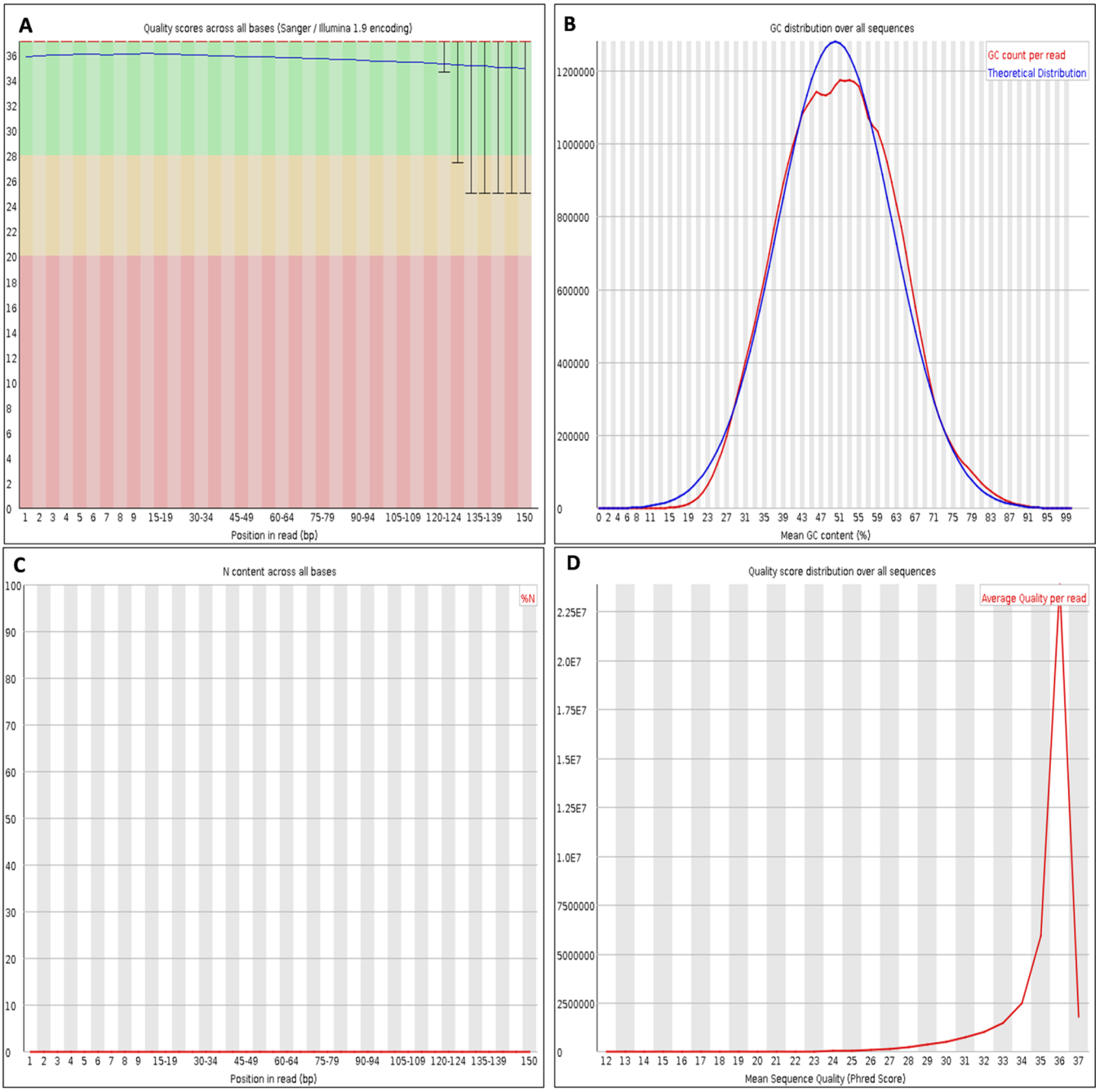

Figure 1. FasQC report of SRA data. (A) Quality/scores across all bases; (B) GC distribution over all sequences; (C) content of bases across all bases; (D) phred score (mean sequence quality).

simulation to run.[26] The docked complex of the best and common ligand with the protein having the highest dock and MMGBSA score was selected for the MD simulations and then compared with the control drug (doxorubicin for 5GWK; etoposide for 4OQ3) using Desmond force field (OPLS 2005). The checkpoint interval of the simulation trajectory was kept at 240.06 ps.

2.11. Principal Component Analysis (PCA). The stability of the protein−ligand complex can be visualized via principal component analysis. Protein biological function is governed by a change in conformation and its fluctuation as a conformation with the respective ligands in the specific cavity. Functional proteins demonstrate flexibility and rigidity of their constituent residues to different extents. In this study, PCA analysis was done using essential dynamics in Schrodinger, LLC, New York, NY, 2020-4 to visualize and revalidate the flexibility or rigidity of the complex. In PCA analysis, projections of PC1 to PC10 were generated. For graphical representation, projections of PC1 and PC2 of the protein−ligand complex were considered.

2.12. Cell Culture and MTT Assay. MDA-MB-231, a triple-negative breast carcinoma cell (human), was procured from NCCS, Pune. Dulbecco's modified Eagle medium (DMEM) was used to grow MDA-MB-231 cells. The media was supplemented with 4 mM L-glutamine, 50 mg/mL streptomycin, 50 units/mL penicillin, and fetal bovine serum (10% (v/v from PAA Laboratories, Austria)) in a 5% CO_2 incubator at 37 °C.

https://doi.org/10.1021/acsomega.3c03640
ACS Omega 2023, 8, 38025−38037

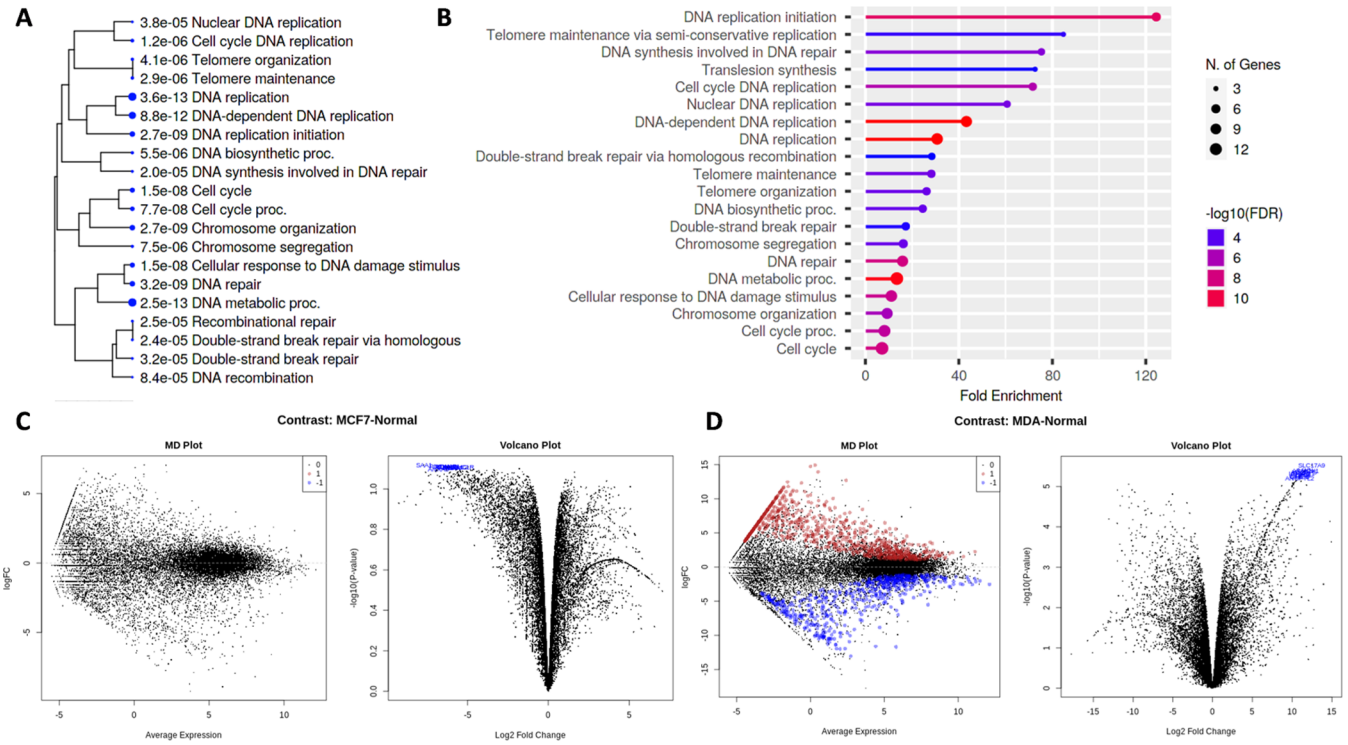

Figure 2. (A–D) Illustration of RNA-Seq analysis to list out DEGs and network generation of closely related upregulated hub genes. (A and B) Tree and fold enrichment of genes associated with similar cellular functions. (C and D) MD and volcano plot of MCF 7 and MDA-MB-231, respectively.

To check the anticancer activity of resveratrol, MTT assay was performed. 1×10^4 cells were seeded overnight in 96-well plates by following the standard cell culture condition stated above. Increasing concentrations (50–140 μM) of the drug were added into the wells and incubated for 56 h. The assay was performed in triplicate for the statistical test. A solution of resveratrol (TCI Chemicals; product number: R0071, CAS RN: 501-36-0) was formed in 100% DMSO and further diluted in serum-free medium (DMEM). After 56 h of treatment, cells were incubated with 3-(4,5-dimethylthiazol-2-yl)-2, 5-diphenyl-2H-tetrazolium bromide (MTT) reagent at a working concentration of 0.5 mg/mL for 3 h. For live cells (due to respiration), the MTT reagent converts to blue formazan crystals, which are insoluble and trapped inside the cells. To solubilize the formazan, 500 μL of DMSO was added into each of the wells. The absorbance of the solution was recorded at 560 nm using a Molecular Devices Spectra Max Plus Plate Reader, while media absorbance was recorded at 690 nm. The value of absorbance is directly proportional to the number of viable cells and was calculated by keeping untreated cells as control.

$$\% \text{ cell viability} = \frac{(\text{OD560} - \text{OD690}) \text{ of treated cells}}{(\text{OD560} - \text{OD690}) \text{ of untreated cells}} \times 100$$

2.13. Western Blotting Analysis. The treated and untreated cells were suspended in the cell lysis buffer (Thermo scientific) and sonicated for 5 min at 4 °C followed by centrifugation (6000 rpm for 10 min) to collect the supernatant. The proteins were separated by sodium dodecyl sulfate-polyacrylamide gel electrophoresis (SDS-PAGE) and transferred onto the polyvinylidene difluoride (PVDF) membranes. The membranes were incubated with primary antibodies, including anti-Akt (1:1000), anti-Map kinase, and anti-β-actin (1:20,000) antibodies overnight. After extensive washing, the membranes were further incubated with the horseradish peroxidase (HRP)-conjugated secondary antibodies for 1 h, followed by reading using an enhanced chemiluminescence detection system.

3. RESULTS AND DISCUSSION

3.1. RNA-Seq and Gene Ontology Analysis. The quality of six untreated human RNA samples retrieved from NCBI (SRR116682386 and SRR116682387 from MCF 10 cell line (as normal), SRR116682394 and SRR116682395 from MCF 7 cell line (sample 1, cancer cell line), and SRR116682402 and SRR116682403 belonging to MDA-MB 231 cell line (sample 2, cancer cell line)) was analyzed using FastQC to generate validated data. Here we used Galaxyweb server to analyze all of the data. Quality scores across all bases, GC content, and phred score were analyzed. The mean value of GC count in the data was observed around 50. Phred scores were observed within the range of 2–40 for all of the data as shown in Figure 1. The data validated were further incorporated for alignment/mapping using the TopHat2 v2.1.1 Galaxyweb server.

We assembled the mapping of reads to generate consensus sequences using the normal MCE 10 sequence data by applying the Bowtie aligner algorithm and generated a BAM file for further feature count analysis. Feature counts of the generated BAM alignment file were incorporated for overlap and exon alignment using htseq (htseq-count script). Furthermore, the data were uploaded for DEG generation using Limma, the Galaxy server. Sample 1 (MCF 7 cell line sample) generated a total of 16,991 (Figure 2C) differentially expressed genes (DEGs), but none of the genes passed the set

https://doi.org/10.1021/acsomega.3c03640
ACS Omega 2023, 8, 38025−38037

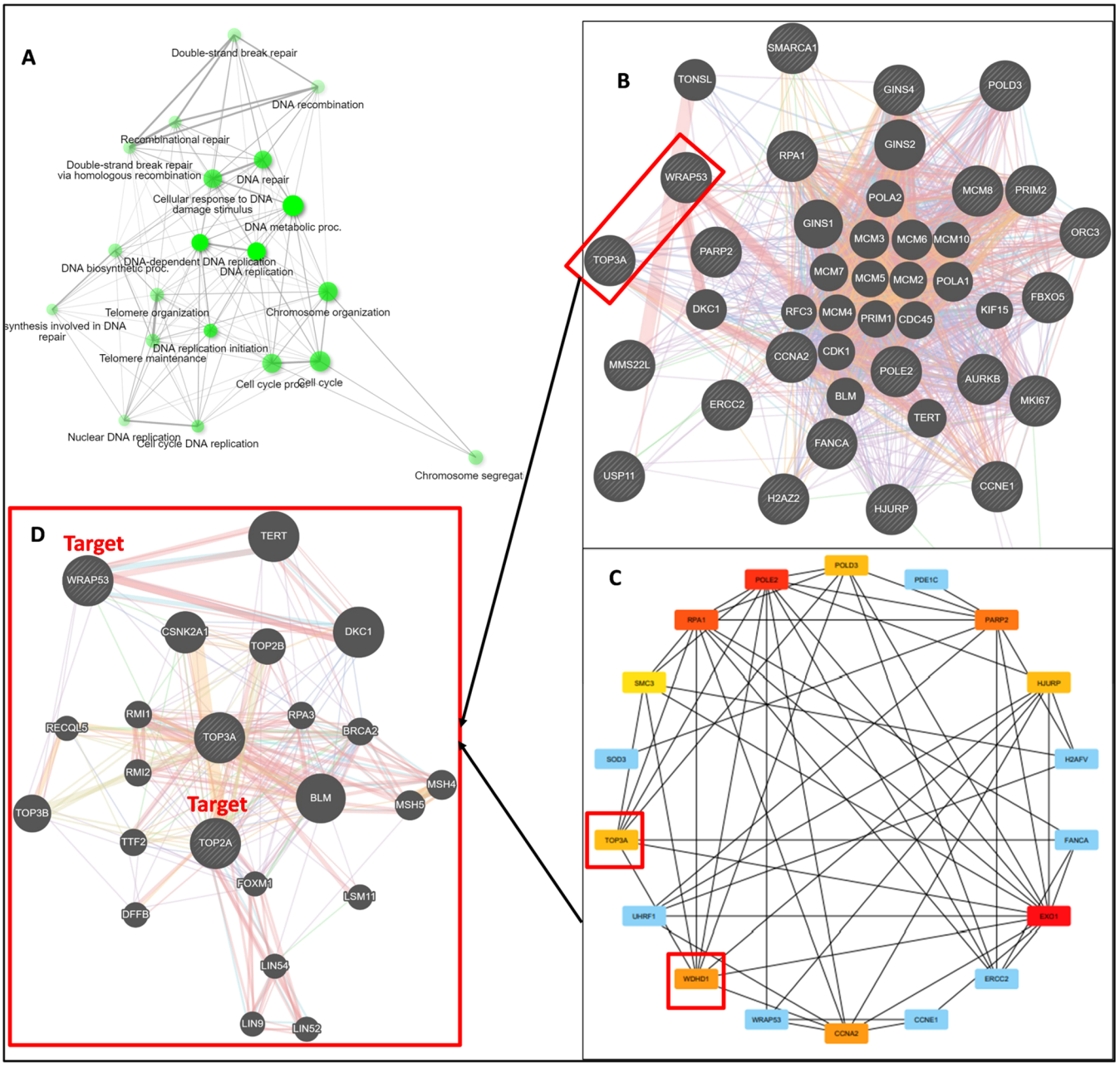

Figure 3. (A) Network of hub genes associated with similar cellular functions; (B–D) closely related network of genes associated with DNA damage/repair/damage stimulus/replication and recombination etc.

threshold value for fold enrichment and p-value. A total of 15,658 differentially expressed genes in sample 2 (MDA-MB 231, triple-negative cancer cell line) were generated using Limma, out of which 808 genes were found to be upregulated (Figure 2D) when the threshold for fold enrichment of >2 and *p*-value of <0.1 were set for filter.

3.2. Hub Gene Identification and Target Protein Selection. To analyze these DEGs, we further did gene ontology studies and generated clusters of genes on the basis of their association with cellular and molecular functions using Bingo and Mcode. We found 35 different clusters of genes. Finally, using cytohubba and GeneMANIA, the 18 best hub genes that are associated with double-strand DNA break, DNA damage, DNA repair, replication, and recombination (as shown in Figure 3) etc. were selected as our target network for further study to find the target proteins.

3.3. Molecular Docking and MMGBSA. Interestingly, it was observed from the network analysis that it contains a total of 18 genes, among which significant genes on the basis of its function in cell arrest/apoptosis like TOP3A and WRAP53 (Figure 3C) are presented. Further, we generated a network of genes associated with these genes (Figure 3D). This is on the basis of the significance of these genes and their expressed proteins in cellular proliferation and growth. Our first target protein, topoisomerase IIα (5GWK), plays an important key role in maintaining the topology of double-helix DNA and results in facilitation of DNA replication and cell division. Our second target protein is the cavity of MDM2 (4OQ3) for p53 to inhibit protein–protein interaction (P53-MDM2) and thus increase the concentration of p53 in the cell, resulting in cell arrest.

https://doi.org/10.1021/acsomega.3c03640
ACS Omega 2023, 8, 38025−38037

For our further study we conducted high-throughput virtual screening (HTVS) of all four prepared libraries (total 1179 ligands) against both target proteins (5GWK and 4OQ3). Out of 1179 ligands screened against both proteins, we selected 15 best ligands against 5GWK and 13 best ligands against 4OQ3, whose docking and MMGBSA scores were lower than the docking and MMGBSA scores of doxorubicin and etoposide, respectively, as control drugs (Tables S1, S2 and Table 1). The lower docking and MMGBSA scores potentially suggest that the ligands bind more strongly with the respective proteins when compared with doxorubicin.

3.3.1. Common Ligand for Topoisomerase IIα (5GWK) and p53-MDM2 (4OQ3) on the basis of Docking and MMGBSA Analysis. From the above screened 15 ligands in the case of 5GWK and 13 in the case of 4OQ3, we found resveratrol (Pubchem ID 5056) as the common ligand in both the selected lists. The docking and MMGBSA scores of resveratrol against 5GWK are −8.606 and −81.76 kcal/mol, respectively, which are lower than those of doxorubicin (as mentioned above). Doxorubicin (PubChem ID 31703) forms a hydrogen bond with ASP463, PRO485*, and DA12(DNA). Residues SER763* and SER464* are involved in polar interaction, and residues such as LEU486*, PRO485*, PHE484, ILE438, PRO439, and MET762* are involved in hydrophobic interaction. Similarly, resveratrol (PubChem ID 5056) interacts with topoisomerase IIα and DNA. It is observed that resveratrol interacts with the active site of topoisomerase IIα, similar to doxorubicin. Resveratrol forms a hydrogen bond with SER763 and DC8(DNA). It also forms pi−pi interaction with (DC8) DNA. Residues like THR460, SER464, HIE758, and HIS759 are involved in polar interaction, and residues like MET762, LEU764, MET765, MET766, ILE490, LEU486, PRO485, ALA465, and TYR757 are strongly involved in hydrophobic interaction. Interestingly, we observe that all of these interacting residues are part of the active site of topoisomerase IIα and the interacting residues are also common in the case of doxorubicin and resveratrol. This strongly suggests that resveratrol can be more effective and less toxic as it is a plant product.

Further, in the case of 4OQ3, the docking and MMGBSA score of resveratrol is −5.315 kcal/mol and −40.38 kcal/mol (Table 1), respectively, which is lower than that of the control drug (Table 1). Comparing the protein−ligand interaction, we observe that etoposide against 4OQ3 forms a hydrophobic interaction with ILE61*, MET62*, LEU57*, PHE55*, LEU54*, ILE19, PHE91*, and VAL93, and residues like GLN59*, GLN24, GLN18, GLN72*, HIE73*, and HIS96* form a polar interaction with a docking score of −4.853 kcal/mol and an MMGBSA score of −50.52 kcal/mol. However, resveratrol also interacts in the same cavity of p53. Resveratrol forms a hydrogen bond with VAL93 and residues like HIS73*, GLN72*, GLN59*, SER92, and HIS96* are strongly involved in forming a polar interaction in the same cavity where p53 binds. Residues TYR60, ILE61*, MET62*, LEU57*, TYR56, PHE55*, LEU54*, VAL75, ILE74, and PHE91* are involved in hydrophobic interaction. Here, the highlighted and star-marked residues are common interacting residues. The interaction of resveratrol with 4OQ3 also supports our aim of finding a common ligand and can be considered for further analysis of validation using MD simulation and PCA analysis to investigate the protein−ligand complex's stability.

3.4. ADME/T Analysis of Best-Screened Ligand (Resveratrol; PubChem ID 5056) and Doxorubicin

Table 1. Docking and MMGBSA Scores of the Best and Common Ligand Against Topoisomerase IIα (5GWK) and p53-MDM2 Protein-Protein Interacting Cavity (4OQ3)

protein PDB ID	ligands PubChem ID	ligand name	docking score (kcal/mol)	MMGBSA DG bind (kcal/mol)	MMGBSA DG bind coulomb (kcal/mol)	MMGBSA DG bind covalent (kcal/mol)	MMGBSA DG bond H bond (kcal/mol)	MMGBSA DG bind solvent (kcal/mol)	interacting residues
5GWK (topoisomerase IIα)	5056	resveratrol	−8.606	−81.76	−88.15	3.52	−1.69	97.66	H bond; SER763, DC8. Polar interaction: THR460, SER464, HIE758, HIS759. Pi−Pi interaction: DC8. Hydrophobic interaction: MET762, LEU764, MET765, MET766, ILE490, LEU486, PRO485, ALA465, TYR757
5GWK (topoisomerase IIα)	31703	doxorubicin	−7.271	−38.41	−37.87	8.26	−0.23	59.52	H bond; ASP463, PRO485, DG10, DA12. Polar interaction: SER763, SER464. Hydrophobic interaction: LEU486, PRO485, PHE484, ILE438, PRO439, MET762
4OQ3 (p53-MDM2)	5056	resveratrol	−5.315	−40.38	−8.53	0.62	−0.14	15.32	H bond: VAL93. Polar interaction: HIS73, GLN72, GLN59, SER92, HIS96. Hydrophobic interaction: TYR60, ILE61, MET62, LEU57, TYR56, PHE55, LEU54, VAL75, ILE74, PHE91
4OQ3 (p53-MDM2)	36462	etoposide	−4.853	−50.52	−0.03	1.1	−0.33	17.86	Polar interaction: GLN24, GLN18, HIE73, GLN72, GLN59, HIS96. Hydrophobic interaction: MET62, ILE61, LEU57, PHE55, LEU54, ILE19, PHE91, VAL93

https://doi.org/10.1021/acsomega.3c03640
ACS Omega 2023, 8, 38025−38037

(PubChem ID 31703). ADME/T property analysis is an essential requirement for any molecule to be considered a lead/drug molecule. Here we observe that all of the three molecules almost come within the range of the ADME/T score (given in Table 2). However, when we observe minutely, we notice that the values for QPCaco and QPPMDCK of resveratrol are fairly better than those of doxorubicin. Resveratrol is found in lots of plant species and has a history of inhibiting replication of the herpes simplex virus.[27] At the same time, it is small in molecular weight, almost half that of doxorubicin. Doxorubicin also has a lot of solubility problems in water and causes heart problems.

3.5. Molecular Dynamics Simulation and PCA Analysis of Resveratrol against 5GWK and 4OQ3.

The simulation study and analysis of resveratrol (PubChem ID 5056) showed appreciable results with both the proteins when compared with the control drugs. During simulation trajectory analysis, protein−ligand interaction has also been observed in the cavity of topoisomerase IIα and the MDM2 cavity of p53 (p53-MDM2).

3.5.1. Molecular Dynamics Simulation and PCA Analysis of Resveratrol against 5GWK. For 5GWK with doxorubicin, the root-mean-square deviation (RMSD) graph demonstrated that the protein and ligand are stable but seem to fluctuate a little with increase in time (Figure 4C). The simulation event analysis (SEA) and protein−ligand interaction during the simulation also support the same. The RMSD means for the Cα chain, side chain, and ligand (doxorubicin) were 5.062 ± 0.651, 5.749 ± 0.657, and 1.121 ± 0.071 Å, respectively. The maximum RMSD deviation for the Cα chain, side chain, and ligand (6.270, 6.894, and 1.353 Å, respectively) also suggested that doxorubicin interacts effectively in the cavity of 5GWK. The fluctuation in Cα chain is not less, as it ranges maximum up to 6.270 Å whereas the mean is also not less, it is 5.062 Å. In case of the side chain also fluctuation ranges maximum up to 6.894 Å. The PCA analysis states that PC1 ranges from −60 to +80 whereas PC2 ranges from −60 to +100.

However, when we did the analysis for 5GWK with resveratrol, the root-mean-square deviation (RMSD) graph demonstrated that the protein and ligand are stable throughout the trajectory of 100 ns and we also observed the decrease in fluctuation after 60 ns (Figure 4H). The simulation event analysis (SEA) and protein−ligand interaction during the simulation also potentially support the same. The RMSD means for the Cα chain, side chain, and ligand (resveratrol) were 4.391 ± 0.635, 5.191 ± 0.652, and 0.377 ± 0.108 Å, respectively, which are also comparatively less. The maximum RMSD deviation during 100 ns of trajectory for the Cα chain, side chain, and ligand (5.639, 6.442, and 0.966 Å, respectively) also suggested that resveratrol interacts effectively in the cavity of 5GWK with more stability when compared with doxorubicin. Other simulation analyses like protein root-mean-square fluctuations (RMSF), and ligand RMSD/RMSF/rGyr/SASA/PSA and B factor also support the above findings (Figures S1 and S2). The PCA analysis also supports the above fluctuation in case of resveratrol (relatively less). The PC1 for resveratrol ranges from −60 to +60, whereas PC2 ranges from −40 to +40. Thus, we can infer from the simulation and PCA data analysis that resveratrol is comparatively more potent and also would exhibit less cytotoxicity on account of being bioactive in nature.[28]

3.5.2. Molecular Dynamics Simulation and PCA Analysis of Resveratrol against 4OQ3. In the case of 4OQ3 with

Table 2. ADME/T Scores of the Best and Common Ligand Against Topoisomerase IIα (5GWK) and p53-MDM2 Protein-Protein Interacting Cavity (4OQ3) Compared with Doxorubicin

s.no	PubChem ID	QP logs	CIQP logs	QPlogHERG	QPPCaco	QPlogBB	QPPMDCK	mol_MW	rule of five	dipole	SASA	FOSA	FISA	PISA
1	36462	−3.405	−5.392	−4.639	205.123	−1.562	89.273	588.564	0	6.905	770.321	505.761	177.569	86.99
2	31703	−2.433	−4.022	−6.061	+2.557	−2.917	0.864	543.526	0	6.443	777.114	316.979	314.779	145.357
3	5056	−2.803	−3.396	−5.333	277.019	−1.293	123.56	228.247	0	3.328	482.183	14.572	163.808	303.803
ADME/T permissible range		−6−(−0.5)	−6.5−(−0.5)	below (−5)	<25 poor >500 great	−3−(−1.2)	<25 poor >500 great	130−725	closet to 5	1−12.5	300−1000	0−750	7−330	0−450

https://doi.org/10.1021/acsomega.3c03640
ACS Omega 2023, 8, 38025−38037

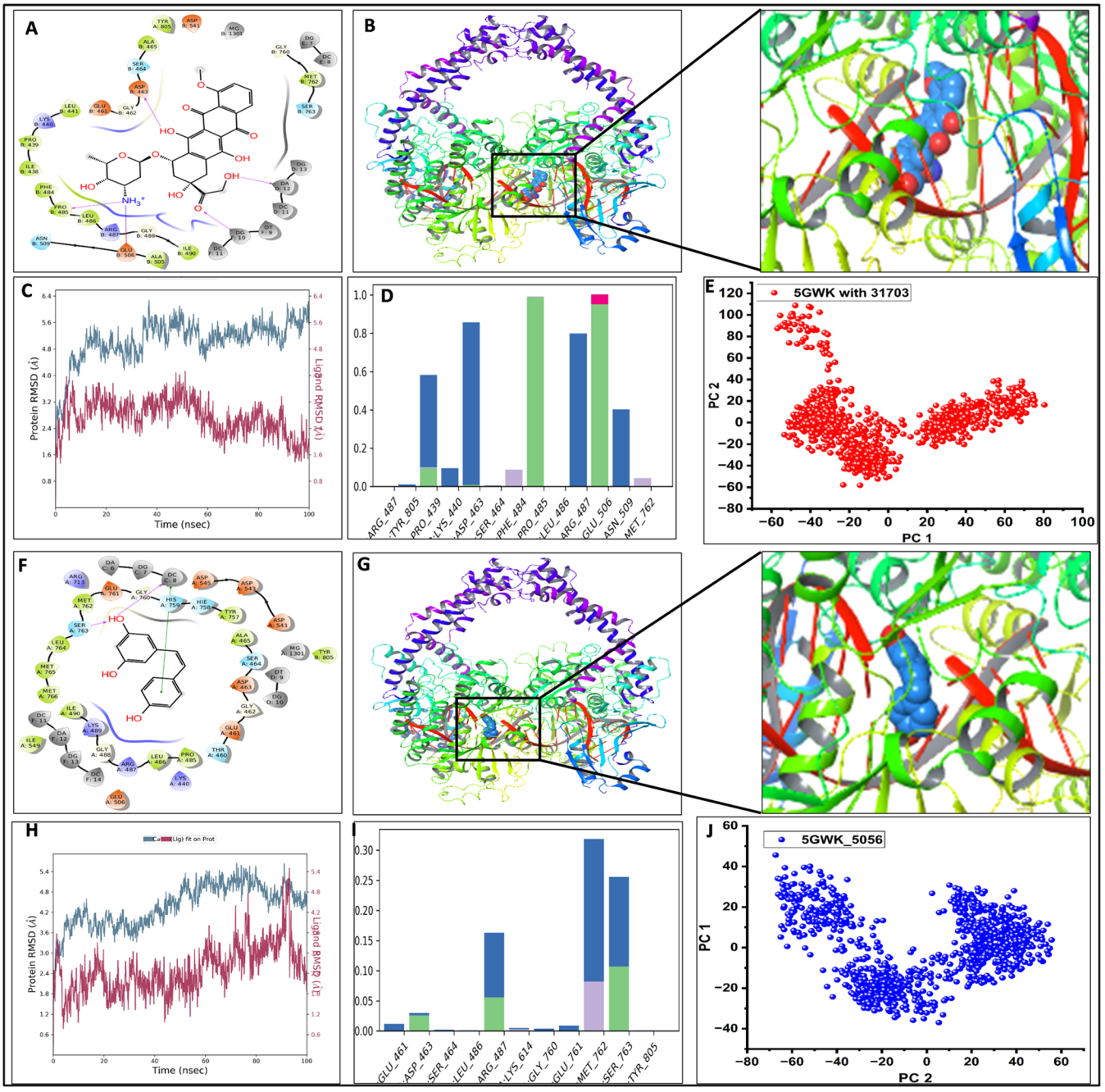

Figure 4. (A) 2D interaction of 5GWK with 31703; (B) 3D interaction of 5GWK with 31703; (C) RMSD plot of 5GWK with 31703; (D) interaction fraction plot of 5GWK with 31703; (E) PCA analysis plot of 5GWK with 31703; (F) 2D interaction of 5GWK with 5056; (G) 3D interaction of 5GWK with 5056; (H) RMSD plot of 5GWK with 5056; (I) interaction fraction plot of 5GWK with 5056; (J) PCA analysis plot of 5GWK with 5056.

etoposide, the root-mean-square deviation (RMSD) graph demonstrated that the protein and ligand are stable and fluctuation is not much. The RMSD means for the Cα chain, side chain, and ligand for etoposide were 1.394 ± 0.284, 3.027 ± 0.344, and 1.654 ± 0.473 Å, respectively, which show that the complex is stable. The maximum RMSD deviation for the Cα chain, side chain, and ligand (2.060, 3.743, and 2.338 Å, respectively) is also not as much as that for etoposide. Further, the PCA analysis states that PC1 ranges from −20 to +10 whereas PC2 ranges from −20 to +18.

Further, MD simulation results of 4OQ3 with resveratrol were analyzed, and it showed better results when compared to the control drug. The RMSD plot of the complex clearly showed a lesser fluctuation in RMSD. The RMSD plot shows stability in fluctuation throughout the simulation time of 100 ns, which can be observed parallel to the *x* axis. This strongly suggests that 4OQ3 is more stable with resveratrol than etoposide (Figure 5H). The simulation event analysis (SEA) and protein−ligand interaction during the simulation also validate the result. The RMSD means for the Cα chain, side chain, and ligand (resveratrol) were 1.132 ± 0.181, 2.500 ± 0.212, and 1.034 ± 0.198 Å, respectively, which are also less than those of control. The maximum RMSD deviation during 100 ns of trajectory for the Cα chain, side chain, and ligand is

https://doi.org/10.1021/acsomega.3c03640
ACS Omega 2023, 8, 38025−38037

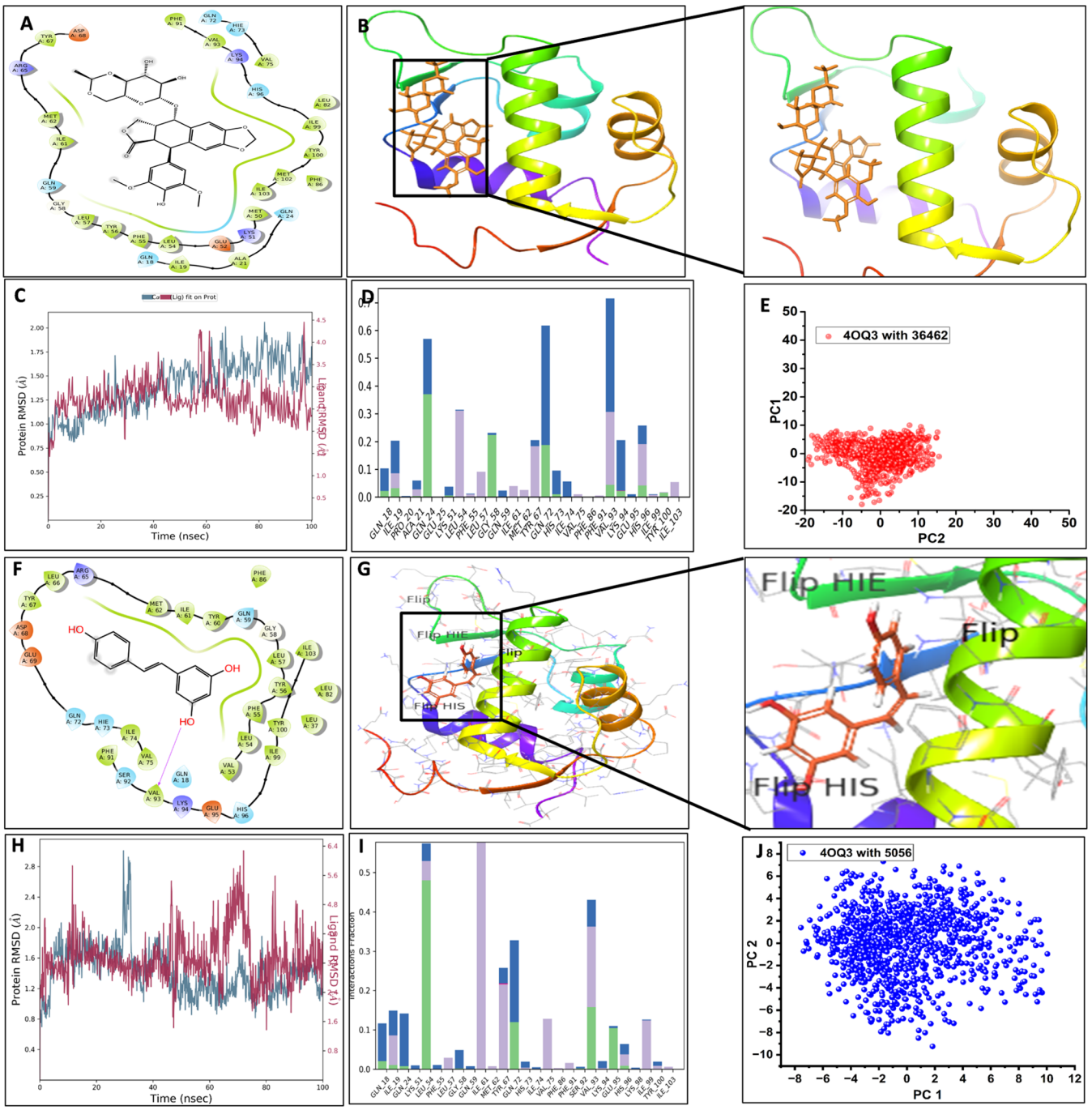

Figure 5. (A) 2D interaction of 4OQ3 with 36462; (B) 3D interaction of 4OQ3 with 36462; (C) RMSD plot of 4OQ3 with 36462; (D) interaction fraction plot of 4OQ3 with 36462; (E) PCA analysis plot of 4OQ3 with 36462; (F) 2D interaction of 4OQ3 with 5056; (G) 3D interaction of 4OQ3 with 5056; (H) RMSD plot of 4OQ3 with 5056; (I) interaction fraction plot of 4OQ3 with 5056; and (J) PCA analysis plot of 4OQ3 with 5056.

1.634, 2.812, and 1.013 Å, respectively. Further analysis and comparison of other parameters like protein RMSF, ligand RMSD/RMSF, rGyr, and B factor of resveratrol with 4OQ3 supports the above observation (Figures S3 and S4). The PCA analysis also validates and advocates the above result. The PC1 for resveratrol ranges from −08 to +10, whereas PC2 ranges from −10 to +07, which states that the fluctuation in the complex is very less when compared with etoposide. Thus, it may be inferred from the simulation and PCA data analysis that resveratrol is comparatively more potent against 4OQ3.

3.5.3. MTT Assay Study. Further, for validation of the above result, we conducted MTT assay to check the cell viability. The MDA-MB 231 cell line is a triple-negative breast cancer, which shows the typical hallmarks of cancer; one of them is cell proliferation. Cells were treated with increasing concentrations of resveratrol (50−140 μM) in triplicates; a medium without resveratrol was added in the control wells. At 56 h post drug treatment, MTT assay was performed (Figure 6). The absorbance of the solution was recorded at 560 nm to measure and compare the number of viable cells in resveratrol-treated and untreated cells as control. The IC_{50} calculated was found

https://doi.org/10.1021/acsomega.3c03640
ACS Omega 2023, 8, 38025−38037

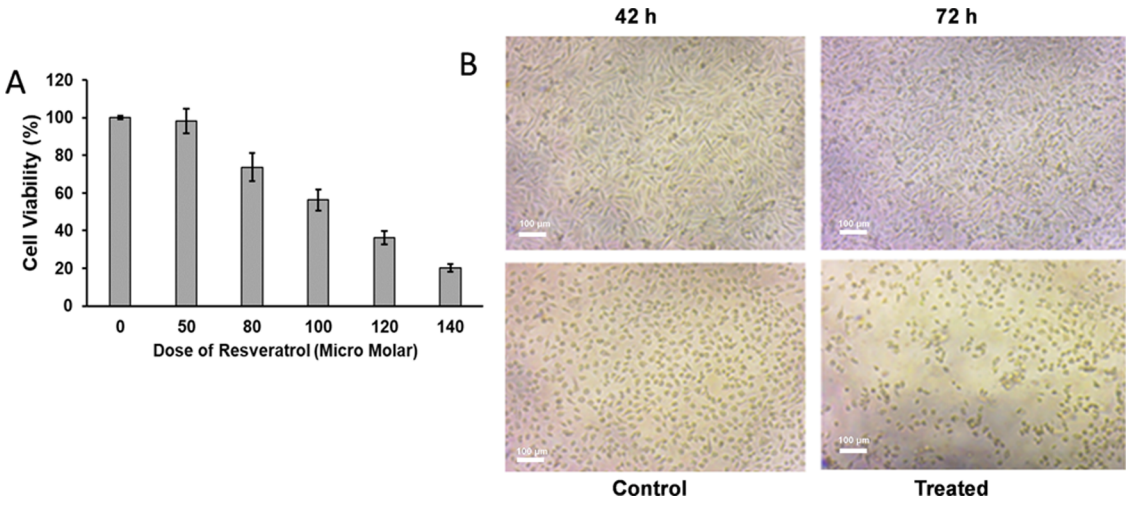

Figure 6. (A) TNBC cells after treatment with resveratrol. The values are represented as the mean ± SD of results from three individual experiments. The IC_{50} value of the drug was 105 ± 10 μM. MTT assay showing the cell viability of MDA-MB-231. (B) Microscopy study of MDA-MB-231 (TNBC) cells with treatment of resveratrol, showing decrease in cell number and change in cellular morphology. Scale bar 100 μm.

to be 105 ± 10 μM. The morphology of 72 h.a.t. as compared to control and 42 h.a.t. show time-dependent cell death, which supports the antitumor activity of resveratrol at IC_{50}.

Moreover, the Akt and MAPKinase gene expressions play a significant role, which supports proliferation as well as cell survival in TNBC as per previous studies. Western blots of Akt and MAPKinase gene expression were compared with untreated (without resveratrol) and treated (with resveratrol) samples. The sample treated with resveratrol showed down-regulation of Akt and MAPKinase as compared to the untreated Akt and MAPKinase samples. Overall, the results indicated that the treated cells showed downregulation of Akt and MAPKinase expression, which possibly led to apoptosis-mediated cell death as compared to untreated cells.

4. CONCLUSIONS

In brief, the results showed that 808 genes were upregulated out of 15658 DEGs in a triple-negative breast cancer cell line (MDA-MB-231). All of these 808 genes were classified into 35 clusters with similar cellular/molecular function, whereas the cluster having 18 genes associated with DNA damage/repair/related function was considered for further analysis. Finally, topoisomerase IIα (5GWK) and p53-MDM2 (4OQ3) genes as well as their corresponding proteins were taken as potential targets. To opt for an effective lead suitable for multitarget therapy, 1179 ligands were screened from various libraries. The docking/MMGBSA/ADMET/MD simulation and PCA results showed that resveratrol, a plant-based bioactive molecule, is the best ligand against both the target proteins. The results for our first target protein (5GWK) were as follows: the RMSD means for the Cα chain, side chain, and ligand for doxorubicin were 5.062 ± 0.651, 5.749 ± 0.657, and 1.121 ± 0.071 Å, respectively, and the PCA analysis shows that PC1 ranges from −60 to +80 and PC2 ranges from −60 to +100. However, for resveratrol, the RMSD means for Cα chain, side chain, and ligand were 4.391 ± 0.635, 5.191 ± 0.652 and 0.377 ± 0.108 Å, respectively, which are also comparatively less. The PC1 and PC2 are also less for resveratol (PC1: −60 to +60 and PC2: −40 to +40). Similarly, for the second target protein (4OQ3), the RMSD means for the Cα chain, side chain, and ligand for etoposide were 1.394 ± 0.284, 3.027 ± 0.344, and 1.654 ± 0.473 Å, respectively. The PCA analysis states that PC1 ranges from −20 to +10 whereas PC2 ranges from −20 to +18. The RMSD mean for the Cα chain, side chain, and ligand (resveratrol) were 1.132 ± 0.181, 2.500 ± 0.212, and 1.034 ± 0.198 Å, respectively. Further, the PC1 for resveratrol ranges from −08 to +10, whereas PC2 ranges from −10 to +07, which states that the fluctuation in the complex is much less when compared with etoposide. MD simulation and PCA analysis for 4OQ3 clearly suggest that resveratrol binds in the cavity with good binding affinity and the ligand seems stable with the protein. This was also evident from the in vitro validation in case of the triple-negative breast cancer cell line MDA-MB-231 via MTT assay and Western blotting analysis. The viability and morphology of cells compared to control showed time-dependent cell death, which supports the antitumor activity of resveratrol at IC50 (105 μM). Therefore, the present study demonstrated that resveratrol may be suitable for multi-targeting therapy against triple-negative breast cancer that has limited options of therapeutics and thus demands urgent development of new therapeutics.

■ ASSOCIATED CONTENT

Supporting Information

The Supporting Information is available free of charge at https://pubs.acs.org/doi/10.1021/acsomega.3c03640.

The SI having Docking and MMGBSA scores of best 15 ligands against topoisomerase IIα (5GWK). Docking and MMGBSA scores of 13 best ligands against p53-MDM2 complex (4OQ3) MD simulation study analysis of 5GWK with doxorubicin MD simulation study analysis of 5GWK with resveratrol MD simulation study analysis of 4OQ3 with doxorubicin MD simulation study analysis of 4OQ3 with resveratrol Western Blotting data showing the decrease in protein band intensity of AKT1 and MAPKinase (MAPK1) (PDF)

■ AUTHOR INFORMATION

Corresponding Authors

Pritish Kumar Varadwaj − *Department of Applied Sciences, Indian Institute of Information Technology Allahabad,*

https://doi.org/10.1021/acsomega.3c03640
ACS Omega 2023, 8, 38025−38037

Allahabad 211015 Uttar Pradesh,, India; orcid.org/0000-0001-5706-2411; Email: pritish@iiita.ac.in

Amaresh Kumar Sahoo − *Department of Applied Sciences, Indian Institute of Information Technology Allahabad, Allahabad 211015 Uttar Pradesh,, India;* orcid.org/0000-0002-9014-3317; Email: asahoo@iiita.ac.in

Authors

Vishal Singh − *Department of Applied Sciences, Indian Institute of Information Technology Allahabad, Allahabad 211015 Uttar Pradesh,, India*

Suman Verma − *Department of Biotechnology, Rani Durgavati Vishwavidyalaya, Jabalpur, Madhya Pradesh 482001, India*

Fiza Fatima − *Department of Molecular and Cellular Engineering, Jacob Institute of Biotechnology and Bioengineering, Sam Higginbottom University of Agriculture, Technology and Sciences, Allahabad 211007 Uttar Pradesh, India*

Sintu Kumar Samanta − *Department of Applied Sciences, Indian Institute of Information Technology Allahabad, Allahabad 211015 Uttar Pradesh,, India;* orcid.org/0000-0002-2695-4043

Complete contact information is available at: https://pubs.acs.org/10.1021/acsomega.3c03640

Notes

The authors declare no competing financial interest.

■ ACKNOWLEDGMENTS

This work also received financial support from Seed Grant of IIIT Allahabad. The authors acknowledge the financial support from DBT, Govt. of India (SAN. No. BT/PR40544/COD/139/14/2020).

■ REFERENCES

(1) Foulkes, W. D.; Smith, I. E.; Reis-Filho, J. S. Triple-Negative Breast Cancer. *N. Engl. J. Med.* **2010**, *363* (20), 1938−1948.

(2) Khazaei-Poul, Y.; Mirmotalebisohi, S. A.; Zali, H.; Molavi, Z.; Mohammadi-Yeganeh, S. Identification of MiR-3182 and MiR-3143 Target Genes Involved in The Cell Cycle as a Novel Approach in TNBC Treatment: A Systems Biology Approach. *Chem. Biol. Drug Des.* **2022**, *101*, 662−677.

(3) Ameri, A.; Tavakoli-Far, B.; Rostami, M.; Abedi kiasari, B.; Sakhaei, D.; Saad Ahmed, O.; Forouzani, F.; Fazli, Y. Recent Advances in Atezolizumab-Based Programmed Death-Ligand 1 (PD-L1) Blockade Therapy for Breast Cancer. *Int. Immunopharmacol.* **2022**, *113*, No. 109334.

(4) Shinohara, H.; Kobayashi, M.; Hayashi, K.; Nogawa, D.; Asakawa, A.; Ohata, Y.; Kubota, K.; Takahashi, H.; Yamada, M.; Tokunaga, M.; Kinugasa, Y.; Oda, G.; Nakagawa, T.; Onishi, I.; Kinowaki, Y.; Kurata, M.; Ohashi, K.; Kitagawa, M.; Yamamoto, K. Spatial and Quantitative Analysis of Tumor-Associated Macrophages: Intratumoral CD163-/PD-L1+ TAMs as a Marker of Favorable Clinical Outcomes in Triple-Negative Breast Cancer. *Int. J. Mol. Sci.* **2022**, *23* (21), 13235.

(5) Serrano-Quintero, A.; Sequeda-Juárez, A.; Pérez-Hernández, C. A.; Sosa-Delgado, S. M.; Mendez-Tenorio, A.; Ramón-Gallegos, E. Immunogenic Analysis of Epitope-Based Vaccine Candidate Induced by Photodynamic Therapy in MDA-MB-231 Triple-Negative Breast Cancer Cells. *Photodiagn. Photodyn. Ther.* **2022**, *40*, No. 103174.

(6) Löscher, W. Single-Target Versus Multi-Target Drugs Versus Combinations of Drugs With Multiple Targets: Preclinical and Clinical Evidence for the Treatment or Prevention of Epilepsy. *Front. Pharmacol.* **2021**, *12*, No. 730257.

(7) Brasnyó, P.; Molnár, G. A.; Mohás, M.; Markó, L.; Laczy, B.; Cseh, J.; Mikolás, E.; Szijártó, I. A.; Mérei, Á.; Halmai, R.; Mészáros, L. G.; Sümegi, B.; Wittmann, I. Resveratrol Improves Insulin Sensitivity, Reduces Oxidative Stress and Activates the Akt Pathway in Type 2 Diabetic Patients. *Br. J. Nutr.* **2011**, *106* (3), 383−389.

(8) Colín-Lozano, B.; Estrada-Soto, S.; Chávez-Silva, F.; Gutiérrez-Hernández, A.; Cerón-Romero, L.; Giacoman-Martínez, A.; Almanza-Pérez, J.; Hernández-Núñez, E.; Wang, Z.; Xie, X.; Cappiello, M.; Balestri, F.; Mura, U.; Navarrete-Vazquez, G. Design, Synthesis and in Combo Antidiabetic Bioevaluation of Multitarget Phenylpropanoic Acids. *Molecules* **2018**, *23* (2), 340.

(9) Li, J.; Yu, H.; Wang, S.; Wang, W.; Chen, Q.; Ma, Y.; Zhang, Y.; Wang, T. Natural Products, an Important Resource for Discovery of Multitarget Drugs and Functional Food for Regulation of Hepatic Glucose Metabolism. *Drug Des., Dev. Ther.* **2018**, *12*, 121−135.

(10) Giordano, S.; Petrelli, A. From Single- to Multi-Target Drugs in Cancer Therapy: When Aspecificity Becomes an Advantage. *Curr. Med. Chem.* **2008**, *15* (5), 422−432.

(11) Proschak, E.; Stark, H.; Merk, D. Polypharmacology by Design: A Medicinal Chemist's Perspective on Multitargeting Compounds. *J. Med. Chem.* **2019**, *62* (2), 420−444.

(12) Hevener, KirkE.; Verstak, T. A.; Lutat, K. E.; Riggsbee, D. L.; Mooney, J. W. Recent Developments in Topoisomerase-Targeted Cancer Chemotherapy. *Acta Pharm. Sin. B* **2018**, *8* (6), 844−861.

(13) Malina, J.; Vrana, O.; Brabec, V. Mechanistic Studies of the Modulation of Cleavage Activity of Topoisomerase I by DNA Adducts of Mono- and Bi-Functional PtII Complexes. *Nucleic Acids Res.* **2009**, *37* (16), 5432−5442.

(14) Hadlaczky, G.; Praznovszky, T.; Sófi, J.; Udvardy, A. Intracellular Forms of *Drosophila* Topoisomerase II Detected with Monoclonal Antibodies. *Nucleic Acids Res.* **1988**, *16* (21), 10013−10023.

(15) Vos, S. M.; Tretter, E. M.; Schmidt, B. H.; Berger, J. M. All Tangled up: How Cells Direct, Manage and Exploit Topoisomerase Function. *Nat. Rev. Mol. Cell Biol.* **2011**, *12* (12), 827−841.

(16) Roca, J.; Wang, J. C. The Capture of a DNA Double Helix by an ATP-Dependent Protein Clamp: A Key Step in DNA Transport by Type II DNA Topoisomerases. *Cell* **1992**, *71* (5), 833−840.

(17) Berger, J. M.; Gamblin, S. J.; Harrison, S. C.; Wang, J. C. Structure and Mechanism of DNA Topoisomerase II. *Nature* **1996**, *379* (6562), 225−232.

(18) Valkov, N. I.; Sullivan, D. M. Tumor P53 Status and Response to Topoisomerase II Inhibitors. *Drug Resistance Updates* **2003**, *6* (1), 27−39.

(19) Wang, S.; Zhao, Y.; Aguilar, A.; Bernard, D.; Yang, C.-Y. Targeting the MDM2−P53 Protein−Protein Interaction for New Cancer Therapy: Progress and Challenges. *Cold Spring Harbor Perspect. Med.* **2017**, *7* (5), No. a026245.

(20) Flatten, K.; Dai, N. T.; Vroman, B. T.; Loegering, D.; Erlichman, C.; Karnitz, L. M.; Kaufmann, S. H. The Role of Checkpoint Kinase 1 in Sensitivity to Topoisomerase I Poisons. *J. Biol. Chem.* **2005**, *280* (14), 14349−14355.

(21) Gupta, A.; Shah, K.; Oza, M. J.; Behl, T. Reactivation of P53 Gene by MDM2 Inhibitors: A Novel Therapy for Cancer Treatment. *Biomed. Pharmacother.* **2019**, *109*, 484−492.

(22) Arriola, E. L.; Lopez, A. R.; Chresta, C. M. Differential Regulation of P21waf-1/Cip-1 and Mdm2 by Etoposide: Etoposide Inhibits the P53-Mdm2 Autoregulatory Feedback Loop. *Oncogene* **1999**, *18* (4), 1081−1091.

(23) Afgan, E.; Baker, D.; Batut, B.; van den Beek, M.; Bouvier, D.; Čech, M.; Chilton, J.; Clements, D.; Coraor, N.; Grüning, B. A.; Guerler, A.; Hillman-Jackson, J.; Hiltemann, S.; Jalili, V.; Rasche, H.; Soranzo, N.; Goecks, J.; Taylor, J.; Nekrutenko, A.; Blankenberg, D. The Galaxy Platform for Accessible, Reproducible and Collaborative Biomedical Analyses: 2018 Update. *Nucleic Acids Res.* **2018**, *46* (W1), W537−W544.

(24) Law, C. W.; Chen, Y.; Shi, W.; Smyth, G. K. Voom: Precision Weights Unlock Linear Model Analysis Tools for RNA-Seq Read Counts. *Genome Biol.* **2014**, *15* (2), R29.

(25) Liu, R.; Holik, A. Z.; Su, S.; Jansz, N.; Chen, K.; Leong, H. S.; Blewitt, M. E.; Asselin-Labat, M.-L.; Smyth, G. K.; Ritchie, M. E. Why Weight? Modelling Sample and Observational Level Variability Improves Power in RNA-Seq Analyses. *Nucleic Acids Res.* **2015**, *43* (15), e97.
(26) Jorgensen, W. L.; Chandrasekhar, J.; Madura, J. D.; Impey, R. W.; Klein, M. L. Comparison of Simple Potential Functions for Simulating Liquid Water. *J. Chem. Phys.* **1983**, *79* (2), 926−935.
(27) Annunziata, G.; Maisto, M.; Schisano, C.; Ciampaglia, R.; Narciso, V.; Tenore, G.; Novellino, E. Resveratrol as a Novel Anti-Herpes Simplex Virus Nutraceutical Agent: An Overview. *Viruses* **2018**, *10* (9), 473.
(28) Thomas, A.; Perry, T.; Berhane, S.; Oldreive, C.; Zlatanou, A.; Williams, L. R.; Weston, V. J.; Stankovic, T.; Kearns, P.; Pors, K.; Grand, R. J.; Stewart, G. S. The Dual-Acting Chemotherapeutic Agent Alchemix Induces Cell Death Independently of ATM and P53. *Oncogene* **2015**, *34* (25), 3336−3348.

https://doi.org/10.1021/acsomega.3c03640
ACS Omega 2023, 8, 38025−38037